

# **ORIGINAL ARTICLE**





# Changes to the lambda model for fatigue loads on steel railway bridges in Europe

Johan Maljaars<sup>1,2</sup> | Stefan Verdenius<sup>1</sup>

#### Correspondence

Prof.dr.ir. Johan Maljaars TNO, Department of Reliable Structures Molengraaffsingel 8 2629 JD Delft The Netherlands Email: johan.maljaars@tno.nl

<sup>1</sup> TNO, Delft, The Netherlands <sup>2</sup> Eindhoven University of Technology, Eindhoven, The Netherlands

#### **Abstract**

For the fatigue design of steel railway bridges in Europe, the European standards EN 1991-2 and EN 1993-2 provide a factored Load Model '71, called the lambda model. The stress range in the fatigue detail of study should be determined with this model. Engineers can easily verify their structural design for fatigue by comparing this stress range to the fatigue reference strength of the detail.

This paper compares the load effect caused by the lambda model with the load effect of actual trains measured with 'Weigh In Motion' systems during 7 years at 81 locations in the rail network of The Netherlands. Locations with heavy loads are selected and their load effects in terms of stress ranges and fatigue damage are determined for various influence lines, including one, two and three span beams with spans ranging between 1 and 150 m. The design (i.e. elastic section modulus) is optimized such that the calculated fatigue damage using the damage accumulation rule of Palmgren Miner equals 1 for a 100 years design life for these locations. This elastic section modulus is compared to the elastic section modulus obtained by designing according to the lambda model.

Improvements are proposed to the lambda model based on this comparison, such that the resulting design gives a reasonable agreement with the design based on measured loads, while maintaining the current ease of use of the lambda model. Uncertainties such as possible changes in axle loads and train speeds in future are taken into account.

#### **Keywords**

Fatigue, Railway bridges, Rail traffic, Lambda model, Weigh in motion

# 1 Introduction

Fatigue is an important design driver for steel and composite steel-concrete railway bridges. A proper fatigue design requires knowledge about the fatigue resistance of the details in a bridge, knowledge about the fatigue loads, and a sufficiently detailed structural model to estimate load effects (i.e. stress ranges) from loads. This paper is about the fatigue loads on railway bridges.

Fatigue is induced by rail traffic. The European standard EN 1991-2 [1] provides two load models for the fatigue design of steel and steel-concrete brides. The most simple of these two, which is further referred to as lambda model, is the subject of the current paper. The load in this model (LM71) is composed of four 250 kN concentrated loads spaced 1.6 m, and a uniformly distributed load of 80 kN/m away from these concentrated loads. The largest bending moment range  $\Delta M_{71}$  (or shear force range) is computed as the difference in moment when applying LM71 on the positive and the negative parts of the influence line (Fig. 1). The stress range  $\Delta \sigma_{71}$  is the bending moment (or shear force) range divided by the section modulus (or shear

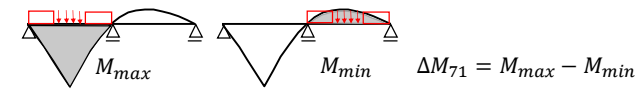


**Figure 1** Application of LM71 to determine  $\Delta M_{71}$ .

area). This range is subsequently multiplied with a number of factors. The multiplicative factors are a partial factor  $\gamma_{Ff}$ , a dynamic factor (DAF)  $\Phi$  and a load effect factor  $\lambda$ :

$$\Phi = \frac{1.44}{\sqrt{L_{\phi} - 0.2}} + 0.82 \text{ but } 1 \le \Phi \le 1.67$$
 (1)

$$\lambda = \min(\lambda_1 \lambda_2 \lambda_3 \lambda_4, \lambda_{max}) \tag{2}$$

$$\lambda_2 = (T/(25 \cdot 10^6 [\text{tonnes}]))^{1/m_2}$$
 (3)

$$\lambda_3 = (t/100[\text{yr}])^{1/m_2}$$
 (4)

$$\lambda_4 = \left(n_s + (1 - n_s) \left(\frac{\Delta \sigma_1}{\Delta \sigma_{1+2}}\right)^{m_2} + (1 - n_s) \left(\frac{\Delta \sigma_2}{\Delta \sigma_{1+2}}\right)^{m_2}\right)^{1/m_2} \tag{5}$$

where  $L_{\Phi}$  is the span (with some correction [1]), T is the annual summed mass of all trains at the track,  $m_2$  is the slope parameter of the long-life part of the S-N curve, t is the design life,  $n_s$  is the fraction of traffic that crosses the

© 2023 The Authors. Published by Ernst & Sohn GmbH.

ce/papers 6 (2023), No. 3-4

bridge simultaneously in bridges accommodating two traffic directions,  $\Delta\sigma_{1+2}$  is the stress range resulting from LM71 on both tracks, and  $\Delta\sigma_1$  and  $\Delta\sigma_2$  are the stress ranges resulting from LM71 on the single track.  $\lambda_1$  is a calibration factor that is dependent on the influence line shape and span and  $\lambda_{max}$  is a maximum value related to the fatigue limit that is not adopted further in this paper. The resulting factored stress cycle must be equal to or smaller than the design fatigue resistance at  $2\cdot 10^6$  cycles,  $\Delta\sigma_C/\gamma_{Mf}$ :

$$\Delta \sigma_{71} \gamma_{Ff} \lambda \Phi \le \Delta \sigma_C / \gamma_{Mf} \tag{6}$$

This lambda model has been established decades ago. Train traffic has changed significantly since that time. Hence, there is a need to verify the appropriateness of the load model for todays and future traffic. In order to do so, a comparison is made in this paper between the load model and actual measured loads obtained through Weigh In Motion (WIM). Possible improvements of the load model are highlighted based on the results.

### 2 Methods and models

WIM appears suited for axle load data of actual traffic [2-5]. WIM systems are installed on almost all tracks in the railway network in The Netherlands. Out of these, 81 tracks are selected for which an almost complete dataset is available over the period of study, 2012 to 2019 (i.e. before the corona pandemic). The characteristics per track differ significantly, with an annual transported mass varying between 2 and 32 million tons per year per traffic direction. The data and the theoretical fatigue damage of each track are described, analysed and visualised in [6]. Based on that analysis, five tracks are selected which are heavily fatigue-loaded but differ significantly in traffic characteristics such as number of axles and fraction of cargo traffic. High speed track is not considered in this work due to a limited amount of available data. The design required for the traffic of these five tracks is compared to the design with the lambda model.

The following calibrations and modifications to the lambda model are studied here, where the asterisk symbol indicates a change to [1]:

$$\Delta \sigma_{71} \gamma_{Ff} \varphi^* (\lambda_1^* \lambda_2 \lambda_3 \lambda_4^* \lambda_5^*) \le \Delta \sigma_C / \gamma_{Mf}$$
 (7)

- Factor  $\lambda_1^*$  is calibrated for a large number of influence lines using the WIM data, with the procedure outlined below. It is displayed as a function of the span instead of a component-specific corrected span as in [1].
- The DAF of Annex D in [1], Eq. (8), is applied instead of Eq. (1) because a comparison with measured data in [7-9] shows that Eq. (8) gives a reasonable upper bound. Factor  $\varphi^*$  uses Eq. (8-9) but with v replaced by  $v^*$  the speed of the single LM71 train where  $v^*$  is calibrated to capture the DAF of trains in the WIM data, each having their own speed v [m/s].
- Factor  $\lambda_4^*$  uses Eq. (5) but with a modified fraction of simultaneous traffic  $n_s^*$  instead of  $n_s$ , where  $n_s^*$  is calibrated to capture the damage contribution of the simultaneous crossings of the actual traffic.
- A trend factor  $\lambda_5^*$  is introduced that considers (possible) future changes in traffic load.

$$\varphi = 1 + \frac{0.5K}{1 - K + K^4} + 0.14 \exp(-L_{\varphi}^2/100[\text{m}^2])$$
 (8)

$$K = \begin{cases} v/160 \text{ [m/s]} & \text{if } L_{\phi} \le 20 \text{ m} \\ v/[\text{m/s}] & \text{if } L_{\phi} > 20 \text{ m} \end{cases}$$
(9)

Software, validated with measured strains in [10], is applied in which the WIM-recorded array of axles with their intermittent (measured) distances is pulled over an influence line and the stress history is recorded, using a trial section modulus (or shear area). A rainflow counting procedure is applied to obtain all stress ranges  $\Delta \sigma_i$  from the stress history. S-N curves with three sets of parameters are considered (Eq. (10) and Table 1) - in accordance with [11] but without a cut-off limit because such a limit has not been proven to exist [12-13]. The fatigue damage D is determined using the linear damage accumulation rule of Palmgren-Miner (Eq. (11)). The elastic section modulus  $W_{el}$  (or shear area) of the influence line is subsequently optimized such that D = 1 over 100 years. The procedure is outlined in Fig. 2, Steps 1 – 5. Fig. 3 shows the influence line shapes considered. The spans considered range between  $1 \text{ m} \le L \le 150 \text{ m}$  for each shape.

$$N_{i} = \begin{cases} N_{D} (\Delta \sigma_{D} / \Delta \sigma_{i})^{m_{1}} & \text{if } \Delta \sigma_{i} \geq \Delta \sigma_{D} \\ N_{D} (\Delta \sigma_{D} / \Delta \sigma_{i})^{m_{2}} & \text{if } \Delta \sigma_{i} < \Delta \sigma_{D} \end{cases}$$
 (10)

$$D = \sum_{i} 1/N_i \tag{11}$$

**Table 1** S-N curve parameters following [11] but without cut-off.

Set	$N_D$	$m_1$	$m_2$
1	5·10 <sup>6</sup>	3	5
2	10 <sup>7</sup>	3	5
3	2·10 <sup>6</sup>	5	9

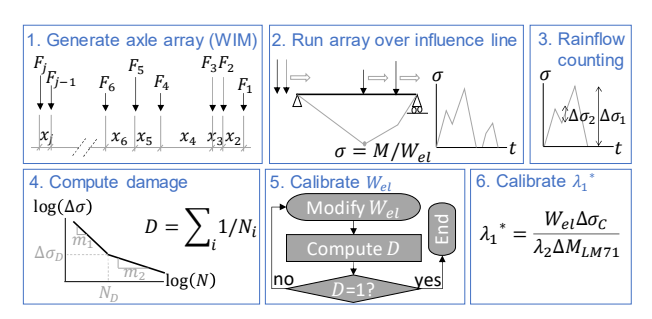


**Figure 2** Outline of the procedure to calibrate  $\lambda_1^*$ .

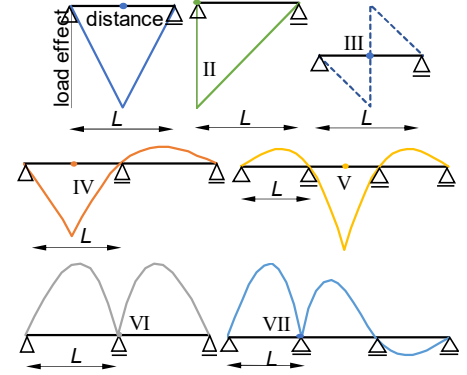


Figure 3 Influence lines considered and their designation (I - VII).

The factor  $\lambda_1^{\ *}$  is calibrated such that a design with it gives

the same  $W_{el}$  as required for the WIM database per track, see Fig. 2 Step 6. The largest required factor over the tracks of study is selected. Subsequently, the speed  $v^*$  of LM71 is calibrated by repeating Steps 1–5 where each axle load in the WIM database is multiplied by Eq. (8) using a speed  $v=v_{rec}+5.6$  [m/s]. The increase of recorded speed  $v_{rec}$  with 5.6 m/s = 20 km/h reflects the expectation that the maximum allowed speeds will increase in the near future. (The maximum allowed speed of cargo and passenger trains on most tracks in The Netherlands is currently 80 km/h and 140 km/h, respectively.) Using Eq. (8-9) again, the single speed  $v^*$  of LM71 is calibrated such that the corresponding factor  $\varphi^*$  equals  $W_{el,\varphi}/W_{el}$ , where  $W_{el,\varphi}$  is the elastic section modulus of Step 5 with each axle multiplied with  $\varphi$  using v.

Fraction  $n_s^*$  is determined by considering the simulations with dual track, using locations where WIM databases are available for both traffic directions. The influence lines of the two tracks are taken identical per simulation. Factor  $\lambda_4^*$  is then determined as:

$$\lambda_4^* = \frac{W_{el,2}}{2W_{el}} \tag{12}$$

where  $W_{el,2}$  is the required elastic section modulus giving a damage of 1 (Steps 1-5 in Fig. 2) if loaded by the joint WIM databases of the two traffic directions. Subsequently,  $n_s^*$  corresponding to  $\lambda_4^*$  is determined using Eq. (5).

Evaluating a number of WIM databases for a long period, it appears that the axle loads have increased and the number of axles have reduced in the last two decades. These findings agree with the qualitative information available about European railways form UIC statistics [14]. The reduced number of axles is most likely related to a replacement of 6 axle cargo wagons by 4 axle cargo wagons and a larger distance between bogies in passenger trains. As a conservative approximation, a negative trend on the number of axles is not considered. Based on the WIM databases, an annual increase factor on the axle load is taken of  $f_{tr}=0.8\%$ , but with a maximization to the allowable maximum axle load of  $F_{ax,max}=250$  kN. A future change in legislation on the maximum axle weight is thus not considered. The axle load in year y,  $F_{ax,y}$ , can then be defined as follows:

$$F_{ax,y} = \min(F_{ax} \cdot (1 + f_{tr}(y - y_0)), F_{ax,max})$$
(13)

where  $F_{ax}$  is the measured axle load and  $y_0$  is the year of measurement. Eq. (13) is applied to all axles in the WIM database. Parameter  $\lambda_5^*$  is then determined as:

$$\lambda_5^* = \frac{\lambda_2 W_{el,tr}}{\lambda_{2,tr} W_{el}} \tag{14}$$

The value of  $W_{el,tr}$  is the value that follows from Step 5 of Fig. 2 for the axle array simulated with  $F_{ax,y}$  and the value of  $\lambda_{2,tr}$  is determined with Eq. (3) using  $T = \sum F_{ax,y}/g$ , where g is the gravity acceleration. Hence, it is the purpose that the effect of the increased annual mass following from the trend is considered through  $\lambda_2$ .

#### Results: modifications to the lambda model

## 3.1 Calibration of $\lambda_1^*$

Fig. 4 shows the computed values for  $\lambda_1^*$  as a function of span L (abscissa) and influence line shape (legend, referring to Fig. 3) for S-N curve 2 (Table 1). The left-hand graph gives the envelope of cargo only tracks and the right-hand graph gives the envelope of mixed (i.e., cargo and passenger) tracks. The span of influence line III is multiplied with a factor of 0.4 in agreement with [1]. As a reference, the factor  $\lambda_1$  according to [1] is added (black).

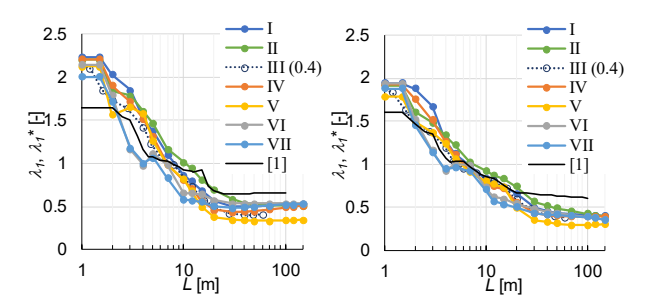


**Figure 4** Calibrated values for  $\lambda_1^*$  (influence lines I – VII) for S-N curve 2, for cargo only track (left) and for mixed traffic track (right).

Fig. 4 shows that  $\lambda_1^*$  varies significantly over span and influence line shape. The shape dependency is caused by the gross representation of actual traffic by LM71, with fixed axle distances and axles embedded in a distributed load.

Comparing cargo only tracks with mixed traffic tracks, it appears that the former require higher factors for  $\lambda_1^*$  except for some influence lines with spans between 10 and 25 m. The larger distances between bogies of passenger trains cause their load effect to be larger in this span range. Double deck trains with their high axle loads contribute more than other passenger train types to the fatique damage.

Fig. 4 also indicates that  $\lambda_1$  according to [1] does not give an upper bound of all influence lines for short spans (L < 20 m). However, this does not necessarily mean that the current lambda model is unconservative, because [1] uses (a) a corrected span for some specific details and (b) a dynamic amplification factor expected to be conservative for short spans. This is elaborated in Section 4.

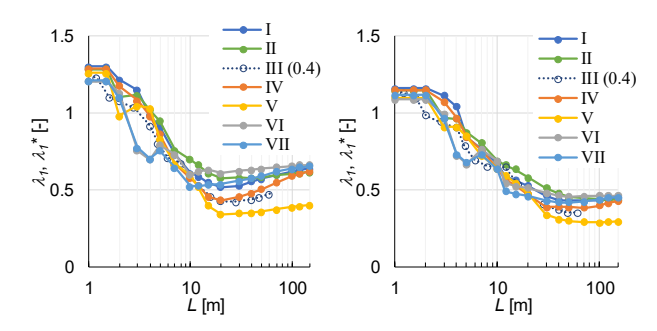


**Figure 5** Calibrated values for  $\lambda_1^*$  (influence lines I – VII) for S-N curve 3, for cargo only track (left) and for mixed traffic track (right).

The results for S-N curve 1 are similar to that of S-N curve 2. It requires 9% lower factors  $\lambda_1^*$  for  $L \leq 3$  m compared to S-N curve 2 and this fraction reduces to 1% for  $L \geq 40$  m. Hence, the results of Fig. 4 can conservatively be used

for S-N curve 1. Fig. 5 gives the results for S-N curve 3. This S-N curve requires lower values for  ${\lambda_1}^*$  compared to the other two S-N curves for short spans ( $L \leq 10$  m), but higher values for long spans ( $L \geq 40$  m).

#### 3.2 Calibration of $v^*$

The calculations show that the dynamic amplification factor  $\varphi^*$  appears almost independent of the S-N curve and the shape of the influence line, but it depends on the traffic type. The dots in Fig. 6 give the results of the simulations using Eq. (8). The figure shows that the variation of  $\varphi^*$  between influence lines is small for cargo only tracks, probably because the variability of speeds between trains is small in these tracks. The variation is slightly larger for mixed traffic tracks.

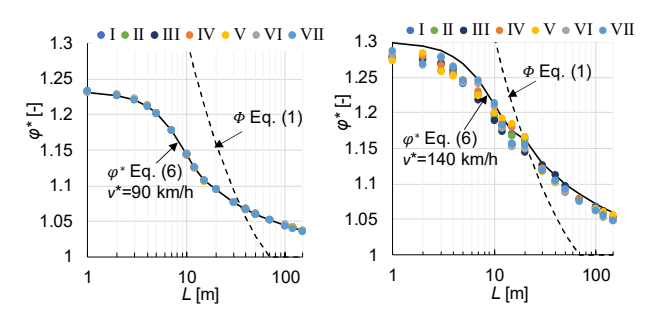


**Figure 6** Calibrated values for  $\varphi^*$  (influence lines I – VII) for cargo only track (left) and for mixed traffic track (right).

Eq. (8) results into a good match with the data if adopting  $v^*=90$  km/h and 140 km/h for cargo only and mixed traffic, respectively, i.e. 10 km/h and 20 km/h lower than the future maximum allowed speeds. This is indicated with the solid curves in the figure.

The dashed curves reflect the standard procedure of the current lambda model in [1], i.e. Eq. (1). A large difference is observed between the two methods. As already mentioned, the former procedure gives a better resemblance of measured data in [6-8] and it is therefore considered an improvement of the lambda model.

## 3.3 Calibration of $n_s^*$

The dots in Fig. 7 present the results of  $\lambda_4^*$  as determined with Eq. (12) - i.e. using the WIM data - for S-N curves 2 (left) and 3 (right) for mixed traffic tracks. The values indicate that the effect of simultaneous crossings increases with increasing span, up to a span of 20 or 50 m. The black lines represent the calculation of  $\lambda_4^*$  using Eq. (5) – i.e. the lambda model – where the fraction  $n_s$  is replaced by  $n_s^*$  and where  $n_s^*$  is calibrated such that  $\lambda_4^*$  provides an upper bound of the calculated effects. As shown in the figure, this results in simultaneous fractions  $n_s^* = 0.03$  and 0.001 for S-N curves 2 and 3, respectively. The fraction of S-N curve 1 is deemed equal to that of S-N curve 2. These results are obtained from WIM systems installed at dual track. However, the cargo trains are generally and on average heavier in one of the two directions, because of freight transport in one direction and empty trains in opposite direction. This may change in future because of a pressure for increased efficiency. A second set of simulations is therefore run where the traffic of both directions is taken equal to that of the heaviest loaded direction. If this would

have been applied as-recorded, the axle loads of the two tracks would pass at exactly the same time, which is unrealistic. For this reason, the database for one of the directions is shifted in the second set of simulations, see Fig. 8, where the distance of 1 km is selected as larger than the longest influence line and the longest trains. It appears that the second set indeed requires slightly larger simultaneous fractions of  $n_s^*=0.04$  and 0.004 for S-N curves 2 and 3, respectively.

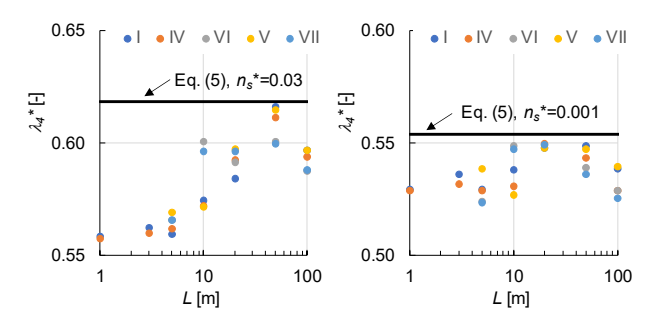


**Figure 7** Calibrated values for  $n_s^*$  (influence lines I and IV – VII) for S-N curve 2 (left) and S-N curve 3 (right).

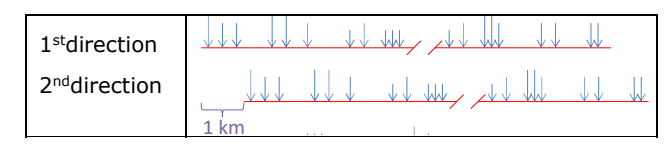
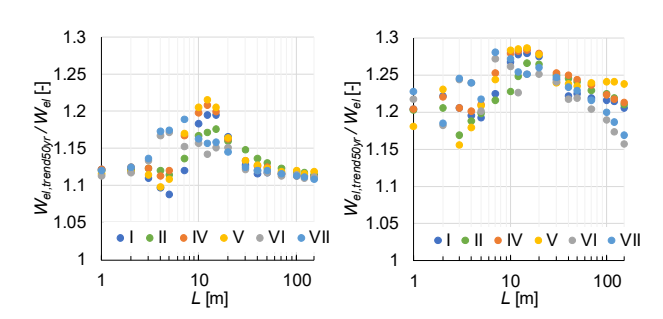


Figure 8 Modified WIM database for 2<sup>nd</sup> direction.

The current value in [1] of  $n_s=0.12$  appears conservative, even though 12% appears close to the actual number of simultaneous crossings in the WIM databases. The lower calibrated value of  $n_s^*$  is related to the low probability of two *very heavy* trains crossing simultaneously (that would contribute considerably to the fatigue damage), since the load model assumes crossings of trains of the same type and weight. Note that the calibrated values for  $n_s^*$  are not representative for locations with a large number of still-standing trains, such as stations.

# 3.4 Calibration of $\lambda_5^*$

The axle load trend effect is evaluated using Eq. (14). Figs. 9 and 10 give intermediate results, by providing the required increase in elastic section modulus for the artificial case that the trends on the individual axles in y=2050 apply for the entire life, i.e. as if the axle weights in the years 2023 to 2123 are at the level of 2050.



**Figure 9** Required increase in elastic section modulus if the trend over 50 years would apply during the entire life for S-N curve 2, for cargo only track (left) and for mixed traffic track (right).

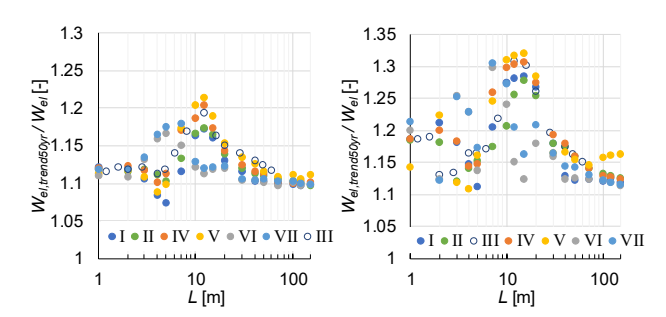


**Figure 10** Required increase in elastic section modulus if the trend over 50 years would apply during the entire life for S-N curve 3, for cargo only track (left) and for mixed traffic track (right).

The largest trend factor is observed for influence line V with  $L=15\,\mathrm{m}$  loaded by mixed traffic. Additional calculations are carried out for this case using other timespans, in each case with axle weights increased with the trend in the last year. These intermediate results are displayed with black dots in Fig. 11. The results of these calculations are subsequently used to determine the lambda trend factor  $\lambda_5^*$  considering the contribution of the trend for each year. Two variants are considered:

- The trend is applied for the entire design life of 100 years: black curve in Fig. 11. The same effect on the damage as obtained with the black curve is created when using a constant value of  $\lambda_5^* = 1.28$  (rounded to 1.3) for S-N curves 1 and 2 and  $\lambda_5^* = 1.33$  (rounded to 1.35) for S-N curve 3. This resulting value comprises the worst case combination of influence line shape and span and it is therefore considered as conservative.
- The trend is applied for the first 50 years and maintained constant thereafter: grey curve in Fig. 11. Background of this variant is that trends for determining static (ULS) loads in [1] are determined for a period of 50 years only. The same effect on the damage is created when using a constant value  $\lambda_5^* = 1.24$  (rounded to 1.25) for S-N curves 1 and 2 and  $\lambda_5^* = 1.27$  (rounded to 1.3) for S-N curve 3.

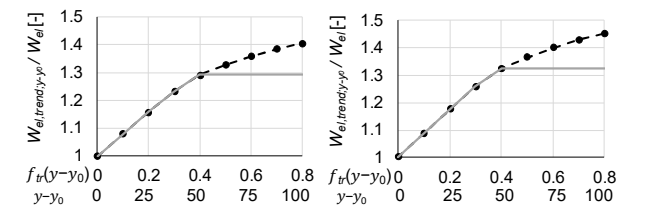


**Figure 11** Elastic section modulus increase determined for various years assuming constant traffic throughout the design life for Influence Line V with L=15 m, for S-N curve 2 (left) and S-N curve 3 (right). Values  $f_{tr}$  refer to Eq. (13).

The resulting  $\lambda_5^*$  factors are relatively large. A more indepth study is required to more realistically estimate trends and simulate trend effects.

# 4 Discussion: comparison of the current lambda model with the new proposed model

To study the accuracy of the current lambda model in [1], the following ratios are considered:

$$r = \frac{\phi \lambda_1}{\varphi^* \lambda_1^*}$$
 and  $r_5 = \frac{\phi \lambda_1}{\varphi^* \lambda_1^* \lambda_5^*}$  (15)

The difference between the ratios is that the latter includes the (uncertain) trend factor on the axle loads. Both ratios consider a bridge with one track only. A ratio > 1 indicates the model in [1] is conservative compared to the data and a ratio < 1 implies it is unconservative. Figs. 12 and 13 give the results for S-N curve 2 and 3, respectively, where the left ordinates give r and the right ordinates give r5. These results for S-N curve 2 are also representative for S-N curve 1.

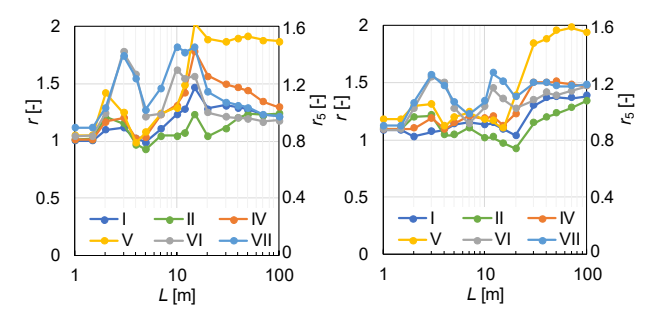


**Figure 12** Accuracy of the lambda model in [1] expressed through ratios r and  $r_{\rm S}$  for S-N curve 2, for cargo only track (left) and for mixed traffic track (right).

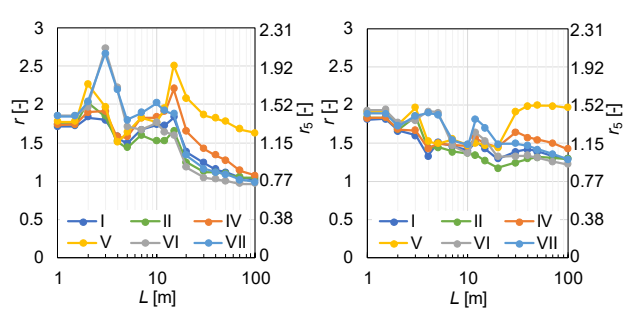


**Figure 13** Accuracy of the lambda model in [1] expressed through ratios r and  $r_5$  for S-N curve 3, for cargo only track (left) and for mixed traffic track (right).

As indicated before, the lambda model in [1] and the model proposed here cannot be compared one-to-one for each influence line because the model in [1] uses a corrected span for some structural components. (This is also the reason why Influence Line III is not shown.) Nonetheless, the large fluctuation of r and  $r_5$  for different spans and influence line shapes indicates that the lambda model in [1] is not so accurate for the design of structures in the tracks of record. Ratio r is equal to or larger than 1 for most spans and influence lines, but it can be very conservative (even more than a factor of 2) for specific influence lines such as a multispan beam. Section 3.1 explains the cause of this. The European standard for concrete bridges, EN 1992-2 [15], gives different sets of  $\lambda_1$  for influence lines of single span beams, end fields of multispan beams, intermediate fields of multispan beams and support regions of multispan beams. Such a distinction matches well with the variation of  $\lambda_1^*$  for different influence line shapes in Figures 4 and 5 (obviously with different lambda values than those in EN 1992-2 [15]).

The lambda model in [1] appears unconservative for many influence lines if considering  $r_5$ . Even though the trends considered here are uncertain, this demonstrates that the

lambda model in [1] is not suited if any change in (average) axle load appears in future.

It should be noted that the model requires a certain level of conservatism to account for uncertainties, e.g., in the approximation of the influence line by practitioners [10, 16]. Applying a similar procedure as in [16], the updated lambda model proposed here requires a partial factor on the load side of  $\gamma_{Ff}=1.1$  to obtain reliabilities in line with the recommended values in EN 1990 [17] (in addition to the recommended partial factors on the resistance side in [11]).

The analyses are based on WIM data of the Dutch railway network. The proposed model needs to be checked with data from tracks of other European countries. However, large differences are not expected because the Dutch cargo traffic is predominantly cross-border and the type of passenger trains are similar in most European countries. High speed track is not considered in the updated model. Considering the train type and speed differences with 'normal' track, a study dedicated to high speed track is recommended.

#### 5 Conclusions

Based on a comparison with extensive WIM databases, this paper studies the adequateness of Eurocode's lambda model for the fatigue design of steel or steel-concrete railway bridges. It appears that the model is not accurate; it can be conservative or unconservative depending on the shape and the span of the influence line and the development of traffic over time. The model can be improved by modifying the train(s) that is (are) used in the model. In lack of such a proposal, this paper presents  $\lambda_1^*$  values as a function of the influence line shape and span. Further, it is proposed to use dynamic amplification factors of Annex D of [1] using a vehicle speed of  $v^*$ =  $v_{max}$  – 10 km/h for cargo only track and  $v^* = v_{max} - 20 \text{ km/h}$  for mixed traffic track, where  $v_{max}$  is the maximum allowed speed (including expected changes in future). In case of dual track bridges, the fraction of simultaneous crossings with LM71 is calibrated as  $n_s^* = 0.04$  for S-N curves with slope parameters  $m_1=3$  and  $m_2=5$  and  $n_s{}^*=0.004$  for S-N curves with  $m_1 = 5$  and  $m_2 = 9$ . Finally, a factor  $\lambda_5^*$  is introduced that accounts for trends in axle loads and a method is developed to calibrate it based on a certain (estimated) annual increase in average axle load.

# Acknowledgements

The authors acknowledge ProRail for supporting this study and for providing the WIM databases.

#### References

- [1] EN1991-2:2003. Eurocode 1: Actions on structures Part 2: Traffic loads on bridges. CEN; 2003.
- [2] Zakharenko, M.; Frøseth, G.T.; Rönnquist, A. Train

- classification using a weigh-in motion system and associated algorithms to determine fatigue loads. Sensors 22 (2022) 1772.
- [3] Hajializadeh, D.; Žnidarič, A.; Kalin, J.; Obrien, E.J. Development and testing of a railway bridge weighin-motion system. Appl Sci 10 (2022) 4708.
- [4] James, G. Analysis of traffic load effects on railway bridges [Ph.D. thesis]. KTH Royal Institute of Technology; 2003.
- [5] Žnidarič, A.; Kalin, J.; Kreslin, M.; Favai, P.; Kolakowski, P. Railway bridge Weigh-in-Motion system. Transp Res Procedia 14 (2016) 4010–4019.
- [6] Verdenius, S.A.; Hengeveld, S.T.; Maljaars, J. New fatigue load models for assessing railway bridges in Europe. Eng Struct 284 (2023) 115914.
- [7] Musser, D.W. Summary of tests on steel girder spans. In: Proc. 59<sup>th</sup> annual convention of the American Railway Engineering Association. vol. 61, 1960, p. 51–78.
- [8] Tobias, D.H. A method for the fatigue evaluation of riveted steel girder railway bridges [Doctoral thesis], University of Illinois at Urbana-Champaign; 1994.
- [9] Mensinger, M.; Fard, R.; Hacker, A.; Näßl, A. Validation of the dynamic amplification factor in case of historic railway steel bridges with short and medium spans. Procedia Eng 156 (2016) 233–240.
- [10] Maljaars, J. Evaluation of traffic load models for fatigue verification of European road bridges. Eng Struct 225 (2020) 111326.
- [11] prEN1993-1-9:2023. Pre-standard Eurocode 3 Design of steel structures – Part 1-9: Fatigue. (March 2023). Brussels: CEN.
- [12] Baptista C, Reis A, Nussbaumer A. Probabilistic SN curves for constant and variable amplitude. Int J Fatigue 101 (2017) 312–27.
- [13] D'Angelo L, Nussbaumer A. Estimation of fatigue SN curves of welded joints using advanced probabilistic approach. Int J Fatigue 97 (2017) 98–113.
- [14] https://uic-stats.uic.org/
- [15] EN 1992-2:2005. Eurocode 2 Design of concrete structures Concrete bridges Design and detailing rules (2005). Brussels: CEN.
- [16] Maljaars J, Leonetti D, Hashemi B, Snijder H. Systematic derivation of safety factors for the fatigue design of steel bridges. Struct Saf 97 (2022) 102229.
- [17] EN 1990:2005. Eurocode Basis of structural design (2005). Brussels: CEN.